# Protocol for Optical-Pumping of $AlH^+$ to a Single Hyperfine State in the Ground Rovibronic Manifold

Panpan Huang,[1] Schuyler Kain,[1] Antonio de Oliveira-Filho,[2] and Brian Odom[1, a)]
[1)] *Department of Physics and Astronomy, Northwestern University, Evanston, IL 60208, USA*
[2)] *Departamento de Qumica, Faculdade de Filosofia, Cincias e Letras de Ribeiro Preto, Universidade de So Paulo, Ribeiro Preto-SP 14040-901, Brazil*

(Dated: 8 July 2020)

In this work we propose an optical pumping scheme to cool trapped $AlH^+$ molecules to the stretched hyperfine state $|F = 7/2, m_F = 7/2\rangle$ of the rovibronic ground state $|X^2\Sigma^+, v = 0, N = 0\rangle$ using a combination of a linearly-polarized and a circularly polarized broadband pulsed laser to cool the rotational degree of freedom and drive the population to the stretched hyperfine state respectively. We find that adding a laser to couple the $v = 1 \rightarrow v = 0$ transition in the $X^2\Sigma^+$ state accelerates the cooling process. We conducted a simulation of the population dynamics by solving rate equations. The hyperfine constants are also calculated to model the hyperfine structure. The results show that under optimum conditions, the population in the stretched hyperfine state of the rovibronic gorund state can reach 63 % after 67.6 µs (334.6 ms) and 95 % after 25.4 ms (1.240 s) with (without) the rovibrational coupling laser.

## I. INTRODUCTION

In recent years, molecules have played increasingly important roles in many applications including precision measurement[1–3], quantum simulation[4], quantum information processing[5,6] and cold chemistry[7,8]. In the measurement of the time variation of $m_p/m_e$, the change of the transition frequency caused by the variation can be enhanced utilizing the nature of sensitivity difference in two internal states of molecules.[1,9–11]. The best upper limit of electric dipole moment (EDM) of electrons today use polar molecules[2] since they could have larger internal electric fields compared to atoms. The rich internal degrees of freedom and the long-range dipole-dipole interaction between polar molecules offer possibilities of developing a quantum toolkit in both quantum simulation and quantum-information processing[12]. Furthermore, the chemical interaction process can be fundamentally controlled by preparing both external and internal states of the reactants[13]. In precision measurement, precise determination of certain transition frequencies by repeatedly driving those transitions is required, and applications such as quantum simulation and quantum chemistry require molecules to be populated in certain pure internal states to exploit the state properties. Therefore, having the ability of fast repeatedly preparing molecules to a pure initial quantum state is essential in these applications.

Deep trap depth of ion trap suppresses the loss caused by collisions with background gas, and often molecular ions can be sympathetically cooled with the co-trapped Doppler-cooled atomic ions, leading to longer trapping lifetime. Therefore, trapped molecular ions are well-suited for applications requires long interrogation time. The controlled cooling of the population in certain hyperfine states of the molecular ion, $HD^+$ has been demonstrated[14]. Rotational cooling was accomplished by optically pumping selected rovibrational transitions[15]. Manipulation of the population at the hyperfine level was then performed by coupling individual hyperfine states within the pumped rovibrational levels. The hyperfine population transferring process took a few tens of seconds to increase the population of the certain hyperfine state by a few percent.

Our group has previously shown that rotational cooling of diatomic molecules can be achieved using only a spectrally-filtered femtosecond laser (SFFL) for species that have relatively large rotational constants and fairly diagonal Frank-Condon factors (FCFs)[16]. One such example is $AlH^+$, where we demonstrated the rotational ground state population increased from a few percent to $\sim$ 95 % within a second[17]. Cooling to a single $M_J$ level was also theoretically investigated using the approach of optimal control theory[18]. However, the problem of cooling to a specified hyperfine state has not yet been addressed. $AlH^+$ has one unpaired electron (electron spin $S = \frac{1}{2}$), and nuclei with nuclear spins $I_1 = \frac{5}{2}$ and $I_2 = \frac{1}{2}$. In the rovibronic state ($N = 0$), since $J = N + S$, $F_1 = J + I_1$, $F = F_1 + I_2$, $AlH^+$ has four hyperfine states which are $F = \frac{3}{2}, \frac{5}{2}$ states for $F_1 = 2$ and $F = \frac{5}{2}, \frac{7}{2}$ states for $F_1 = 3$.

In this article, we proposed a method to transfer the population to a single stretched hyperfine state of the rovibronic ground state in an efficient way. In Section II, we will explain the theory and our method of performing optically driven and laser-enhanced rotational cooling. We then present our design to extend our selectivity and optically pump the system to a single stretched hyperfine state. The simulation details will be described in Section III while Section IV presents our simulation results and discussion. We conclude in Section V.

[a)] Electronic mail: b-odom@northwestern.edu

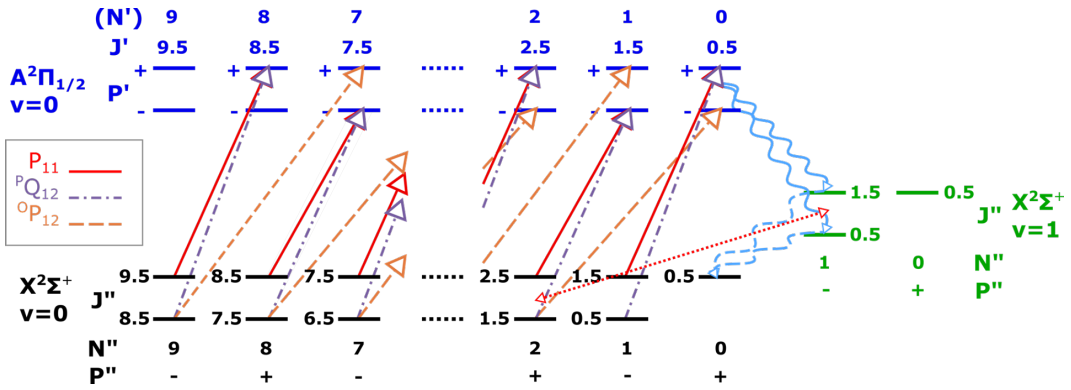


**FIG. 1:** Energy level structure of $AlH^+$ and the rotational cooling scheme. The rotational cooling laser drives $P_{11}$, ${}^PQ_{12}$ and ${}^OP_{11}$ branches from $|X^2\Sigma^+, v = 0\rangle$ to $|A^2\Pi_{1/2}, v = 0\rangle$. Though the rotational angular momentum is not a good quantum number in $A^2\Pi$, $N'$ is used as a convenient label for different J values and transition branches here. The time scale of the electronic relaxation without vibrational excitation from $|A^2\Pi_{1/2}, v = 0\rangle$ to $|X^2\Sigma^+, v = 0\rangle$ is around 0.4 µs. The solid wavy blue arrows represent the electronic spontaneous relaxation with vibrational excitation. The dashed wavy blue arrows represent the rovibrational relaxation within the X state, which happens on the time scale of 140 ms. The rate of population transfer from $v = 1$ to $v = 0$ in the X state is then limited by this time scale, which can be decreased by adding the rovibrational coupling laser, denoted by V10 laser (indicated by the dashed red arrow).

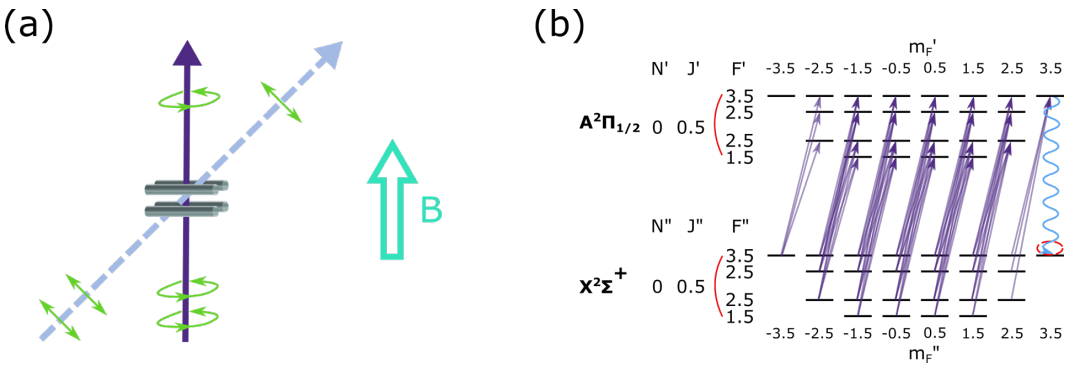


**FIG. 2:** (a) The schematic setup and (b) the hyperfine structure of the rovibrational ground state in $X^2\Sigma^+$ and $A^2\Pi_{1/2}$. In (a), rods of a linear Paul trap and two SFFLs are shown. The dashed light blue arrow represents the linearly polarized SFFL (RC laser) that performs rotational cooling. The solid purple arrow represents the $\sigma^+$-polarized SFFL (HC laser) that drives the $Q_{11}(0)$-branch transition to optically pump the population into the stretched hyperfine state in the ground rovibrational manifold. In (b), the hyperfine structure and the set of transitions driven by the $\sigma^+$-polarized SFFL are shown. The population in the rovibrational ground state in $X^2\Sigma^+$ is driven toward a single dark state, $|X^2\Sigma^+, v = 0, N = 0, F'' = 3.5, m_{F''} = 3.5\rangle$.

## II. THEORY AND METHODS

### A. Rotational Cooling

Our group has previously demonstrated broadband rotational cooling of $AlH^+$ using a linearly-polarized SFFL with 100 fs pulse centered at 360 nm. The pulse is generated from a frequency-doubled femtosecond laser (Spectra-Physics Mai Tai) with 80 MHz repetition rate, so the pulse spectrum is divided into a frequency comb with 80 MHz spacing between neighboring teeth. Its large bandwidth pumps many rotational transitions simultaneously. We use frequency-domain pulse shaping to selectively excite rotational cooling transitions. The vibrational constant is $\sim 1600$ cm$^{-1}$ for $AlH^+$, which is large compared to the bandwidth of the SFFL laser ($\sim 200$ cm$^{-1}$). This permits us to include only $|X^2\Sigma^+, v = 0, 1\rangle$ and $|A^2\Sigma^+, v = 0\rangle$ states when modeling the cooling dynamics.

In the electronic ground state of $AlH^+$, $X^2\Sigma^+$, the various angular momenta of $AlH^+$ are well-described by Hund's case (b), with good quantum numbers $\{\Lambda, N, S, J, P\}$. The $A^2\Pi$ electronic state of $AlH^+$ is better-described using the Hund's case (a) basis of $\{\Lambda, S, \Sigma, J, \Omega, P\}$. Though $N$ is not a good quantum number in $A^2\Pi$, for convenience, we still use $N$ to mark

different J values in the $A^2\Pi$ state (see Figure 1) and label transition branches. It should be noted that the rotational states of both the X and A states of $AlH^+$ have parity doublets. In the X state, the doubling is a result of electron spin-molecular rotation interaction while the doubling in the $A^2\Pi$ state is produced by $\Lambda$ doubling. For both electronic states, $v$ is the vibrational quantum number. We invoke the convention that $v'$ ($v''$) denotes the vibrational quantum number of the upper (lower) state.

As shown in Figure 1, the rotational cooling process has two parts. The first part is a fast cycle in which linearly-polarized 360 nm pulses of the SFFL drive the electronic transition connecting $|X^2\Sigma^+, v'' = 0\rangle$ and $|A^2\Pi_{1/2}, v' = 0\rangle$. Following excitation to the A state, electronic spontaneous emission without vibrational excitation occurs with a relaxation time of $\sim$0.4 µs. Before rotational cooling, significant rotational population is in the lowest ten rotational states. Through the fast cycle, nearly all of it can be driven into the two lowest rotational states, $|v'' = 0, N'' = 0, 1\rangle$, within a few microseconds. However, parity is flipped for a dipole transition such as $|X^2\Sigma^+\rangle \leftrightarrow |A^2\Pi\rangle$. As a result, the population in $|X^2\Sigma^+, v'' = 0, N'' = 1, -\rangle$ cannot be transferred to the rovibronic ground state, $|X^2\Sigma^+, v'' = 0, N'' = 0, +\rangle$ via this fast electronic-cooling cycle which always conserves the parity after an even number of transitions. Nonetheless, the population in $|X^2\Sigma^+, v'' = 0, N'' = 1, -\rangle$ can still transfer to the $|X^2\Sigma^+, v'' = 0, N'' = 0, +\rangle$, but must do so in an odd number of transitions to flip the parity. The shortest parity-flipping process happens in three transitions: first the population in $|X^2\Sigma^+, v'' = 0, N'' = 1, -\rangle$ being excited by the SFFL to the A state, then spontaneous decaying to an intermediate state with negative parity, $|X^2\Sigma^+, v'' = 1, N'' = 1, -\rangle$, and finally going through vibrationally relaxation to reach $|X^2\Sigma^+, v'' = 0, N'' = 0, +\rangle$. This parity-flipping process, which constitutes the second part of the cooling process, is relatively slow because the vibrational relaxation time for the $|X^2\Sigma^+, v = 1\rangle \leftrightarrow |X^2\Sigma^+, v = 0\rangle$ transition is 140 ms.

In our laboratory, $AlH^+$ ions are trapped in a linear Paul trap and initially sympathetically cooled to sub-Kelvin translational temperatures using co-trapped Doppler-cooled $Ba^+$. To remove the dark states of barium ion during the Doppler cooling process, a 2 G magnetic field is applied. After translational cooling, the linearly-polarized SFFL (laser polarization is 45° relative to the direction of the laboratory-applied magnetic field) is turned on to perform rotational cooling of the molecules into their rovibronic ground state.

Rotational cooling of the negative-parity populations is rate-limited by the vibrational-decay timescale. We propose to address this bottleneck through the addition of a 6.7 µm continuous-wave laser which couples the $|X^2\Sigma^+, v'' = 1, N'' = 1, -\rangle \leftrightarrow |X^2\Sigma^+, v'' = 0, N'' = 2, +\rangle$ transition to accelerate part of the parity-flipping process. This technique has not been previously proposed to speed up rotational cooling using broadband lasers. We show the quantitative result from the simulation of accelerating the rotational cooling process with the 6.7 µm continuous-wave laser. The simulation results are shown in Figure 3 and Table V.

### B. Hyperfine Cooling

As we are interested in pumping our system to a single hyperfine quantum state, we also add a circularly-polarized 360 nm beam. By taking advantage of the selection rules for transitions driven by $\sigma^+$-polarized light, we can optical pump the system to a stretched hyperfine state in which the total angular momentum ($F$) has the largest projection ($m_F$) along the quantization axis. The schematic plot of our setup is shown in Figure 2. When we apply the $\sigma^+$-polarized laser, the selection rule are as follows:

$$\Delta F = 0, \pm 1$$
$$\Delta m_F = 1$$

As can be seen in Figure 2, if we park the $\sigma^+$-polarized laser to drive the $Q_{11}(0)$-branch transition[1], $|X^2\Sigma^+, v'' = 0, N'' = 0\rangle \leftrightarrow |A^2\Pi_{1/2}, v' = 0, N' = 0\rangle$, most of the population in the rovibronic ground state of $X^2\Sigma^+$ will be further optically pumped to a single stretched hyperfine state, notably the stretched state of maximal $F$. This stretched hyperfine state is a dark state; it cannot absorb any more $\sigma^+$-polarized photons because there is no higher $m_F$-state available within $|A^2\Pi_{1/2}, v = 0, N = 0\rangle$. Thus the population will accumulate in the stretch state over time. Adding a 6.7 µm continuous-wave laser here also accelerates the hyperfine cooling process. The simulation results are shown in Figure 4 and Table VI.

## III. SIMULATION DETAILS

Our population dynamics are modeled by the following

[1] This notation describes the branch in terms of both $N$ and $J$: ${}^{\Delta N}\Delta J_{ul}$. Note that N is not a good quantum number in $A^2\Pi$, and just serves as a convenient label. If $\Delta N = \Delta J$, then the notation uses one letter to mark the type of branch. $u$ and $l$ denote the spin orientations of the upper and lower states of a transition. In our case, the upper-state could be either $A^2\Pi_{1/2}$ or $A^2\Pi_{3/2}$. These states, corresponding to $|\Omega = \Lambda - 1/2\rangle$ or $|\Omega = \Lambda + 1/2\rangle$, are distinguished as $u = 1$ and $u = 2$, respectively. Analogously, the lower-state, part of the $X^2\Sigma^+$ manifold, has $S = 1/2$. Our convention is that $l = 1$ and $l = 2$ represent $|J = N + 1/2\rangle$ and $|J = N - 1/2\rangle$.

**TABLE I:** Molecular constants for the $X^2\Sigma^+$ state of $AlH^+$ [a]

| Constant[19] | $X^2\Sigma^+$, $v=0$ | $X^2\Sigma^+$, $v=1$ |
|---|---|---|
| $B_v$ | 6.563231 | 6.184845 |
| $D_v \times 10^4$ | 4.5720 | 5.0983 |
| $H_v \times 10^8$ | −0.238 | −6.586 |
| $L_v \times 10^{11}$ | −1.712 | |
| $M_v \times 10^{14}$ | 1.140 | |
| $N_v \times 10^{18}$ | −7.07 | |
| $\gamma_v \times 10^2$ | 5.665 | 5.035 |
| $\gamma_{Dv} \times 10^5$ | −1.896 | −2.09 |
| Origin | 0 | 1523 |

a in $cm^{-1}$

**TABLE II:** Molecular constants for the $A^2\Pi$ state of $AlH^+$ [b]

| Constant | $A^2\Pi$, $v=0$ |
|---|---|
| $B_v$ | 6.727[20] |
| $A_v$ | 108[20] |
| $p_v \times 10^2$ | 1.643[19] |
| $q_v \times 10^3$ | 1.499[19] |
| $D_v \times 10^4$ | −4.14[20] |
| Origin | 27713[19] |

b in $cm^{-1}$

**TABLE III:** Permanent and transition dipole moments ($\langle$ State A $|\,\mu\,|$ State B$\rangle$) [c]

| State A \ State B | $X^2\Sigma^+, v=0$ | $X^2\Sigma^+, v=1$ | $A^2\Pi, v=0$ |
|---|---|---|---|
| $X^2\Sigma^+, v=0$ | −0.389 | | |
| $X^2\Sigma^+, v=1$ | 0.087 | −0.2861 | |
| $A^2\Pi, v=0$ | 1.566 | −0.2806 | −0.928 |

c in Debye

**TABLE IV:** Hyperfine constants of $AlH^+$ in terms of Frosch-Foley coefficients and parameters of nuclear quadrupole interaction[d]

| Constant | $X^2\Sigma^+$ | | $A^2\Pi$ | |
|---|---|---|---|---|
| | Al | H | Al | H |
| a | $1.680 \times 10^{-3}$ | $8.64 \times 10^{-5}$ | $8.511 \times 10^{-3}$ | $5.53 \times 10^{-4}$ |
| b | $3.951 \times 10^{-2}$ | $2.01 \times 10^{-2}$ | $1.382 \times 10^{-2}$ | $-9.35 \times 10^{-3}$ |
| c | $5.039 \times 10^{-3}$ | $2.59 \times 10^{-4}$ | $-5.654 \times 10^{-3}$ | $2.79 \times 10^{-4}$ |
| d | 0 | 0 | $1.040 \times 10^{-2}$ | $4.60 \times 10^{-4}$ |
| $eQq0$ | $-1.341\,211 \times 10^{-3}$ | $2.126\,36 \times 10^{-6}$ | $6.203\,58 \times 10^{-4}$ | $2.342\,31 \times 10^{-6}$ |
| $eQq2$ | 0 | 0 | $-2.896\,52 \times 10^{-3}$ | $-5.633\,15 \times 10^{-7}$ |

d in $cm^{-1}$

system of rate equations:

$$\frac{\partial \rho_i}{\partial t} = -\sum_{j\neq i} B_{i,j}(I_{BBR}+I_{laser})\rho_i - \sum_{j<i} A_{i,j}\rho_i + \sum_{j\neq i} B_{j,i}(I_{BBR}+I_{laser})\rho_i + \sum_{j>i} A_{j,i}\rho_i \quad (1)$$

where $\rho_i$ is the population fraction in state $i$. The initial population is assumed to be thermal with a temperature of 300 K. $I_{BBR}$ and $I_{laser}$ are the energy densities of the blackbody radiation and laser. A and B are the spontaneous emission and stimulated emission Einstein coefficients, respectively.

$$A_{ul} = \frac{2\pi\tilde{\nu}^2 q_e^2}{\epsilon_0 m_e c}\frac{g_l}{g_u} f_{lu}$$
$$B_{ul} = \frac{q_e^2}{4\epsilon_0 m_e h c\tilde{\nu}}\frac{g_l}{g_u} f_{lu} \quad (2)$$
$$B_{lu} = \frac{q_e^2}{4\epsilon_0 m_e h c\tilde{\nu}} f_{lu}$$

In order to determine the Einstein coefficients using Equation (2), we utilize Western's PGOPHER[21] software to compute transition energies and oscillator strengths for $AlH^+$. A 10 G laboratory-frame magnetic field is as-

sumed here to address the problem of the dark states while driving the P-branch rotational cooling transition using a linearly-polarized beam. By adding the magnetic field with an angle between 0 and 90 degrees with respect to the polarization direction of the rotational cooling laser (as shown in Figure 2), dark state evolves on the time scale of Larmor precession. 10 G makes the dark state evolve in $\sim 10^9$ s$^{-1}$, which is sufficiently fast compared to the Rabi frequency of the rotational cooling laser which is on the order of $10^8$ s$^{-1}$ to destabilize the population in the dark state.

We require a number of empirical parameters that describe the states of the $AlH^+$ molecule. Table I and II present the empirical values used throughout this work to describe the $X^2\Sigma^+$ and $A^2\Pi$ states.

Additionally, we use Le Roy's LEVEL[22] to calculate the electric permanent and transition dipole-moments from potential-energy and transition dipole-moment functions of a prior work[23]. These results are presented in Table III.

Dalton[24,25] quantum-computational software was used to compute hyperfine and nuclear-quadrupole coupling constants of the $X^2\Sigma+$ and $A^2\Pi$ states, which are listed in Table IV. We choose the pcJ-1 basis set because pcJ family was developed for RMN/EPR spin-spin coupling constants and have tight functions that are well suited for describing the electron density near the nucleus. Density Functional Theory (DFT) using the B3LYP density functional is applied with an pcJ-1 basis set for all computations.

At room temperature, 99 % of the $AlH^+$ population is in the lowest vibrational state, $v = 0$ within the $X^2\Sigma$ manifold. In turn, within this vibrational ground state, thermal distribution produces significant populations among the first ten J-levels, $J$ = 0.5-9.5, and less than 4 % in $J > 9.5$. Therefore, we include only these lowest ten J-states in our rate-equation simulation for both the X and A states. We also include the $X^2\Sigma^+(v'' = 1)$ manifold so that we can simulate the parity-flipping process via the intermediate state, $|X^2\Sigma^+, v'' = 1, N'' = 1, -\rangle$.

Our femtosecond laser has a frequency-domain representation in the simulation. The spectrum is described by 80 MHz-spaced comb teeth within a Gaussian envelope that is centered at 360 nm and has a ∼7 nm FWHM bandwidth. We model our pulse shaping apparatus as a cut-off filter to the laser spectrum. The cut-off frequency is chosen so as to pass the range of frequencies that selectively drives a set of rotational cooling transitions. For example, we choose to drive the $P_{11}$, ${}^OP_{12}$ and the ${}^PQ_{12}$ branches using the linearly-polarized SFFL and then include the $Q_{11}(0)$ branch for the $\sigma^+$-polarized SFFL. We assume a 200 mW power split equally between the linear- and the $\sigma^+$-polarized beams with a focused 400 µm-diameter spot at the position of $AlH^+$ molecules.

The typical optical transition linewidth for $AlH^+$ is ∼ 20 MHz, which is smaller than the 80 MHz comb-teeth spacing of the femtosecond laser spectrum. As a result, it is possible for the SFFL comb-line to fall outside of the transition linewidths of some of the transitions we desire to drive. We solved this issue in the simulation by introducing a Doppler-broadened linewidth contribution that assumes the translational temperature of the $AlH^+$ ion cloud is ∼1 K. Doing so ensures that there is at least one comb-line within the linewidth of every desired cooling transition. One can accomplish this form of broadening in the experiment by raising the translational temperature of the $AlH^+$ ions in a couple ways. One can excite the secular motion of the $AlH^+$ with an AC field or introduce additional micro-motion by shifting the entire ion cloud away from the geometric center of the Paul trap using a DC field. After internal cooling is finished, one can then turn off the source of translational heating to allow $AlH^+$ to be sympathetic cooled by the laser-cooled $Ba^+$ again.

We simulate the laser-enhanced parity-flipping processes as well. For such cases, we represent the laser (V10) that drives the $|X^2\Sigma^+, v'' = 1, N'' = 1, -\rangle \leftrightarrow |X^2\Sigma^+, v'' = 0, N'' = 2, +\rangle$ transition to match the specifications of a commercial Fabry-Perot quantum-cascade laser from Thorlabs. The laser outputs ∼ 200 mW with ∼15 cm$^{-1}$ bandwidth and could be customized to center at ∼ 6.7 µm to drive the transition of the $v'' = 0 \leftrightarrow v' = 1$ band in the electronic ground state of $AlH^+$.

## IV. RESULT AND DISCUSSION

Figure 3 and Table V present rotational cooling rates for two schemes. In the first scheme, we apply the linearly-polarized rotational cooling laser (RC). In the second scheme, we apply the rotational cooling laser (RC) as well as a laser (V10) that drives the $|X^2\Sigma^+, v'' = 1, N'' = 1, -\rangle \leftrightarrow |X^2\Sigma^+, v'' = 0, N'' = 2, +\rangle$ transition. From Figure 3(a), it can be seen that without V10 laser, the population in the rovitational ground state ($v$,$N$) = (0,0) increases to 45 % within a few µs through the fast rotational cooling cycles. Afterwards, the population in (0,0) keeps increasing but with a slower increasing rate as shown in Figure 3(b). This is because the population accumulated in $|X^2\Sigma^+, v'' = 0, N'' = 1, -\rangle$ experiences the parity flipping process via $|X^2\Sigma^+, v'' = 1, N'' = 1, -\rangle$ with a longer time scale mostly being contributed by the vibrational relaxation time (140 ms) to reach the rovibrational ground state. The addition of the V10 laser reduces the time of the vibrational relaxation process from $|X^2\Sigma^+, v'' = 1, N'' = 1, -\rangle$ to $|X^2\Sigma^+, v'' = 0, N'' = 2, +\rangle$. The time it takes for the population in the rovibronic ground state, $p_0$, to grows to 63 % reduces from 60.0 ms to 8.7 µs. The trend continues as $p_0$ reaches 95 %, which takes only 162.0 µs, also significantly shorter than the 359.4 ms required in the absence of the V10 laser.

Transferring population among hyperfine states was demonstrated in Ref. [14] with $HD^+$. The transferring process took tens of seconds and the population increase in the target hyperfine state was limited to a few percent. In this work, we propose a more efficient hyperfine-

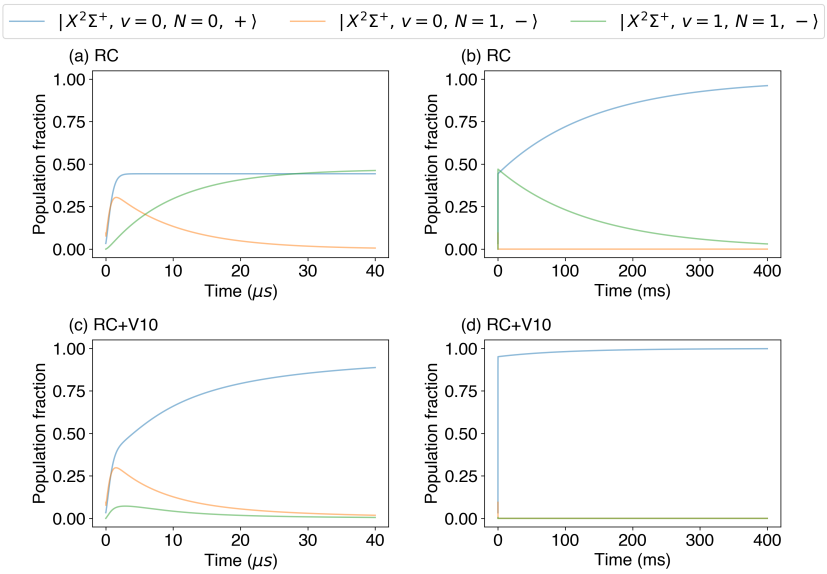


**FIG. 3:** Simulated population dynamics for rotational cooling: The top two plots are for the cases in which only the linearly-polarized rotational cooling SFFL (RC) was applied for (a) 40 µs and (b) 400 ms, respectively. The bottom two plots describe rotational cooling via the SFFL and the additional laser (V10) to drive the $|X^2\Sigma^+, v'' = 1, N'' = 1, -\rangle \leftrightarrow |X^2\Sigma^+, v'' = 0, N'' = 2, +\rangle$ transition, for (c) 40 µs and (d) 400 ms, respectively.

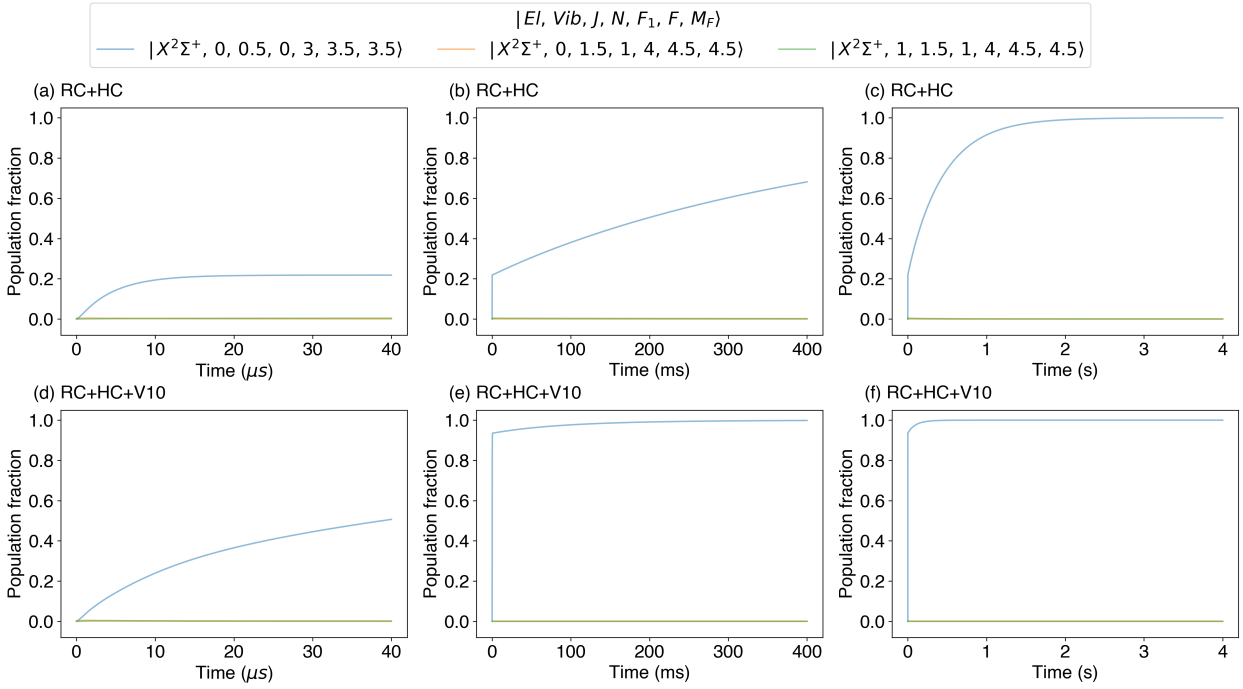


**FIG. 4:** Simulated population dynamics for preparation of a single hyperfine state: The top three plots are for the cases in which the linearly-polarized rotational cooling SFFL (RC) and the $\sigma^+$-polarized hyperfine-cooling SFFL (HC) are applied for (a) 40 µs, (b) 400 ms, and (c) 4 s, respectively. The bottom two plots describe rotational- and hyperfine-cooling via the linearly- and circularly-polarized SFFLs and the additional laser (V10) to drive the $|X^2\Sigma^+, v'' = 1, N'' = 1, -\rangle \leftrightarrow |X^2\Sigma^+, v'' = 0, N'' = 2, +\rangle$ transition, for (d) 40 µs, (e) 400 ms, and (f) 4 s, respectively.

**TABLE V:** The times for the rovibronic ground state population ($p_0$) to reach 63 % and 95 %.

| Laser-fields | 63 % | 95 % |
|---|---|---|
| RC | 60.0 ms | 359.4 ms |
| RC, V10 | 8.7 µs | 162.0 µs |

**TABLE VI:** The time for the hyperfine stretched state population ($p_{0s}$) to reach 63 % and 95 %.

| Laser-fields | 63 % | 95 % |
|---|---|---|
| RC, HC | 334.6 ms | 1240 ms |
| RC, HC, V10 | 67.6 µs | 25.4 ms |

cooling procedure with $AlH^+$. Figure 4 and Table VI present our simulation results for two hyperfine-cooling schemes. In the first scheme, we apply the rotational cooling laser (RC) and the $\sigma^+$-hyperfine-cooling laser (HC). In the second scheme, in addition to the RC laser, we apply the hyperfine-cooling laser (HC) as well as the rovibrational coupling laser (V10). As can be seen in Figure 4(a), in the absence of the V10 laser, the population in the stretched hyperfine state increases to $\sim 20\%$ during the first tens of microseconds via fast rotational cooling cylces and the hyperfine optical pumping cycles. Since the hyperfine cooling process takes additional cycles to transport the population to the stretched state, the time scale is longer compared to the case where only the RC laser is applied. Afterwards, the increasing rate slows down due to the relatively long vibrational relaxation time scale. After a second, the population reaches more than 90 %. From Figure 4(d), we can see that when the V10 laser is also applied, the slow-down effect due to vibrational relaxation is alleviated. The time it takes for the stretched hyperfine-state population in the rovibronic ground state, $p_{0s}$, to reach 63 % is shortened from 334.6 ms to 67.2 µs. If we leave the lasers on, $p_{0s}$ can reach 95 % in 25.4 ms with the V10 laser, a near 50-fold reduction from the 1240 ms in its absence.

## V. CONCLUSION

In order to exploit the full advantage of molecular ion, efficient state preparation is important. We have described a method to achieve faster and more selective internal state cooling in the molecular ion, $AlH^+$. We based our design on the simple premise that in order to speed up the cooling process, we have to accelerate the rate-limiting step. In the $AlH^+$ system, the rate-limiting step is the parity-flipping process. We expect to accomplish this task by adding a new laser field that drives population out of the intermediate state. We further describe an extension to our previous rotational cooling work that should enable one to drive population to a single hyperfine state. We exploit the selection rules of a circularly-polarized laser field in a simulation and find that we should be able to prepare 95 % $AlH^+$ to a single quantum state around a second.


[1] J. Kobayashi, A. Ogino, and S. Inouye, "Measurement of the variation of electron-to-proton mass ratio using ultracold molecules produced from laser-cooled atoms," Nature Communications, vol. 10, no. 1, pp. 1–5, 2019.

[2] V. Andreev and N. Hutzler, "Improved limit on the electric dipole moment of the electron," Nature, vol. 562, no. 7727, pp. 355–360, 2018.

[3] J. Biesheuvel, J.-P. Karr, L. Hilico, K. Eikema, W. Ubachs, and J. Koelemeij, "Probing QED and fundamental constants through laser spectroscopy of vibrational transitions in $HD^+$," Nature Communications, vol. 7, p. 10385, 2016.

[4] K. Ohmori, G. Pupillo, J. H. Thywissen, and M. Weidemüller, "Special issue on addressing many-body problems with cold atoms and molecules," Journal of Physics B: Atomic, Molecular and Optical Physics, vol. 51, no. 2, p. 020201, 2017.

[5] D. D. Susanne F. Yelin and R. Ct, "Quantum information processing with ultracold polar molecules," in Cold Molecules: Theory, Experiment, Applications (R. V. Krems, W. C. Stwalley, and B. Friedrich, eds.), ch. 17, p. 629, CRC Press, 2009.

[6] K.-A. B. Soderberg, N. Gemelke, and C. Chin, "Ultracold molecules: vehicles to scalable quantum information processing," New Journal of Physics, vol. 11, no. 5, p. 055022, 2009.

[7] N. Balakrishnan, "Perspective: Ultracold molecules and the dawn of cold controlled chemistry," The Journal of Chemical Physics, vol. 145, no. 15, p. 150901, 2016.

[8] J. L. Bohn, A. M. Rey, and J. Ye, "Cold molecules: Progress in quantum engineering of chemistry and quantum matter," Science, vol. 357, no. 6355, pp. 1002–1010, 2017.

[9] D. DeMille, S. Sainis, J. Sage, T. Bergeman, S. Kotochigova, and E. Tiesinga, "Enhanced sensitivity to variation of $m_e/m_p$ in molecular spectra," Physical Review Letters, vol. 100, no. 4, p. 043202, 2008.

[10] M. G. Kokish, P. R. Stollenwerk, M. Kajita, and B. C. Odom, "Prospects for a polar-molecular-ion optical probe of varying proton-electron mass ratio," Physical Review A, vol. 98, no. 5, p. 052513, 2018.

[11] P. R. Stollenwerk, M. G. Kokish, D. Oliveira-Filho, G. Antonio, F. R. Ornellas, and B. C. Odom, "Optical pumping of $TeH^+$: Implications for the search for varying mp/me," Atoms, vol. 6, no. 3, p. 53, 2018.

[12] Q. Wei, S. Kais, B. Friedrich, and D. Herschbach, "Entanglement of polar molecules in pendular states," The Journal of Chemical Physics, vol. 134, no. 12, p. 124107, 2011.

[13] M. De Miranda, A. Chotia, B. Neyenhuis, D. Wang, G. Quéméner, S. Ospelkaus, J. Bohn, J. Ye, and D. Jin, "Controlling the quantum stereodynamics of ultracold bimolecular reactions," Nature Physics, vol. 7, no. 6, pp. 502–507, 2011.

[14] U. Bressel, A. Borodin, J. Shen, M. Hansen, I. Ernsting, and S. Schiller, "Manipulation of individual hyperfine states in cold trapped molecular ions and application to $HD^+$ frequency metrology," Physical review letters, vol. 108, no. 18, p. 183003, 2012.

[15] T. Schneider, B. Roth, H. Duncker, I. Ernsting, and S. Schiller, "All-optical preparation of molecular ions in the rovibrational ground state," Nature Physics, vol. 6, no. 4, pp. 275–278, 2010.

[16] C.-Y. Lien, S. R. Williams, and B. Odom, "Optical pulse-shaping for internal cooling of molecules," Physical Chemistry Chemical Physics, vol. 13, no. 42, pp. 18825–18829, 2011.

[17] C.-Y. Lien, C. M. Seck, Y.-W. Lin, J. H. Nguyen, D. A. Tabor, and B. C. Odom, "Broadband optical cooling of molecular rotors from room temperature to the ground state," Nature Communications, vol. 5, no. 1, pp. 1–7, 2014.

[18] A. Aroch, S. Kallush, and R. Kosloff, "Optimizing the multicycle subrotational internal cooling of diatomic molecules," Physical

Review A, vol. 97, no. 5, p. 053405, 2018.
[19] W. Szajna and M. Zachwieja, "High-resolution emission spectroscopy of the $A^2\Pi$–$X^2\Sigma^+$ system of $AlH^+$," Journal of Molecular Spectroscopy, vol. 269, no. 1, pp. 56–60, 2011.
[20] G. Almy and M. Watson, "The band spectrum of ionized aluminum hydride," Physical Review, vol. 45, no. 12, p. 871, 1934.
[21] C. M. Western, "Pgopher: A program for simulating rotational, vibrational and electronic spectra," Journal of Quantitative Spectroscopy and Radiative Transfer, vol. 186, pp. 221–242, 2017.
[22] R. J. Le Roy, "Level: A computer program for solving the radial schrödinger equation for bound and quasibound levels," Journal of Quantitative Spectroscopy and Radiative Transfer, vol. 186, pp. 167–178, 2017.
[23] J. H. Nguyen, C. R. Viteri, E. G. Hohenstein, C. D. Sherrill, K. R. Brown, and B. Odom, "Challenges of laser-cooling molecular ions," New Journal of Physics, vol. 13, no. 6, p. 063023, 2011.
[24] K. Aidas, C. Angeli, K. L. Bak, V. Bakken, R. Bast, L. Boman, O. Christiansen, R. Cimiraglia, S. Coriani, P. Dahle, E. K. Dalskov, U. Ekström, T. Enevoldsen, J. J. Eriksen, P. Ettenhuber, B. Fernández, L. Ferrighi, H. Fliegl, L. Frediani, K. Hald, A. Halkier, C. Hättig, H. Heiberg, T. Helgaker, A. C. Hennum, H. Hettema, E. Hjertenæs, S. Høst, I.-M. Høyvik, M. F. Iozzi, B. Jansík, H. J. Aa. Jensen, D. Jonsson, P. Jørgensen, J. Kauczor, S. Kirpekar, T. Kjærgaard, W. Klopper, S. Knecht, R. Kobayashi, H. Koch, J. Kongsted, A. Krapp, K. Kristensen, A. Ligabue, O. B. Lutnæs, J. I. Melo, K. V. Mikkelsen, R. H. Myhre, C. Neiss, C. B. Nielsen, P. Norman, J. Olsen, J. M. H. Olsen, A. Osted, M. J. Packer, F. Pawlowski, T. B. Pedersen, P. F. Provasi, S. Reine, Z. Rinkevicius, T. A. Ruden, K. Ruud, V. V. Rybkin, P. Sałek, C. C. M. Samson, A. S. de Merás, T. Saue, S. P. A. Sauer, B. Schimmelpfennig, K. Sneskov, A. H. Steindal, K. O. Sylvester-Hvid, P. R. Taylor, A. M. Teale, E. I. Tellgren, D. P. Tew, A. J. Thorvaldsen, L. Thøgersen, O. Vahtras, M. A. Watson, D. J. D. Wilson, M. Ziolkowski, and H. Ågren, "The Dalton quantum chemistry program system," WIREs Comput. Mol. Sci., vol. 4, no. 3, pp. 269–284, 2014.
[25] "Dalton, a molecular electronic structure program," 2018. Release v2018.2 (2018), see `http://daltonprogram.org`.